



Shahid Chamran
University of Ahvaz

Journal of Applied and Computational Mechanics



Research Paper

Design of Centrifugal Fan with Flexible Blades to Extend the Effective Operating Range in Various Speeds and Mass Flows Based on Numerical Analysis and Statistical Computation

Thai Thanh Hiep¹, Le Thanh Long², Vu Viet Thang¹, Hong Duc Thong¹

¹ Department of Automotive Engineering, Faculty of Transportation Engineering, Ho Chi Minh City University of Technology (HCMUT), VNU-HCM, Ho Chi Minh City, Vietnam

² Department of Machine Design, Faculty of Mechanical Engineering, Ho Chi Minh City University of Technology (HCMUT), VNU-HCM, Ho Chi Minh City, Vietnam

Received August 22 2023; Revised March 18 2024; Accepted for publication May 23 2024.

Corresponding author: T.T. Hiep (thaithanhiep@hcmut.edu.vn)

© 2024 Published by Shahid Chamran University of Ahvaz

Abstract. This paper presents research on raising the efficiency and pressure of centrifugal fans at different speed ranges. This problem is related to the incompatibility of the fan characteristics with the speed conditions of the impeller and flow conditions of the installation when the centrifugal fans are operated, which decreases efficiency and raises energy consumption. In this research, a novel concept of regulating the blade parameters of centrifugal fans was given. The basis of this study is that a change in the blade angles and impeller outer diameter at different speeds significantly affects the power and the pressure rise of the fan. The scientific basis of this idea, which is using flexible blades for the fan, is aimed at providing high flow rates at relatively low running speeds, relatively low power requirements, and high efficiency when the fan operates in high-speed regions. Therefore, the design of the fan uses variable angles of the impeller blades by linking each blade to two springs. It enables adjustment to change the inlet and outlet blade angle of the impeller, which allows extending the range of operating parameters in accordance with the impeller speed. The flow simulation tests (CFD) of the novel method demonstrated the feasibility of adjusting the blade parameters and confirmed the benefits of this solution. The results of the research are given on the basis of the numerical analysis method and statistical computation method.

Keywords: Flexible fan blade, adjustable fan blade, centrifugal fan, efficiency, impeller.

1. Introduction

Industrial fans are devices that use the mechanical energy of a rotating impeller to create air movement and increase its total pressure. According to their mechanical design, fans can be divided into two main categories including centrifugal fans and axial fans [1]. Centrifugal fans transport the air by changing its direction in the impeller. Air enters the impeller in the center, turns at a right angle, and then moves radially outward by centrifugal force between the rotary blades of the impeller. There are many studies on centrifugal fans with the aim of increasing efficiency and reducing fan energy consumption. Research by Moczko et al. [2], [3] showed the idea of changing the impeller diameter to change the flow rate and pressure rise of the centrifugal fan. The study used a design with variable lengths of impeller blades, including fixed and movable components enabling modification of the external diameter through the movable blade pushed out or pulled in by the push-pull rod. The idea allowed the fan to extend the effective range and improve operating parameters under different operating conditions. The results of the study by Ding et al. [4] presented that the total pressure and efficiency of the centrifugal fan were significantly impacted by changing the blade outlet angle. By means of computational fluid dynamics (CFD), the characteristics of the fan, including velocity, pressure, and turbulent energy distribution of the centrifugal fan, were collected and compared. Chen et al. [5] studied the performance of a centrifugal fan in a commercial street sweeper. The fan performance and flow field were analyzed by the CFD method, the results showed that the volute and the impeller are major factors influencing flow loss in the fan. Le et al. [6] investigated the effect of speed on the efficiency and flow characteristics of centrifugal fans, the research showed that changes in operating conditions substantially impact fan performance and the pressure maintained within the fan. Bamberger et al. [7][8] presented a quick method for designing efficient centrifugal impellers, the study is based on an evolutionary optimization algorithm that determines the best geometrical parameters for a specific aerodynamic objective function. Improving turbine blades is currently a significant field of research dedicated to developing more efficient gas turbines [9], with the structural performance of the gas turbine rotor and stator blades investigated in this work. Pholdee et al. [10] proposed an ideal sweep blade type for an axial wind turbine utilizing a hybrid surrogate-assisted optimizer. The leading-edge blade curve and pitch angle are regarded as design parameters, and CFD was used



for high-precision simulation to analyze the aerodynamics of the wind turbine blade. Research by Subramanya [11] presented a design fan that meets the requirements for suction static pressure and airflow rate, the study was carried out on the design parameters such as fan diameter, blade outlet angle, number of impeller blades, splitter blade length and diffuser exit length, etc. Roffi et al. [12] developed a new concept of an axial fan with flexible blades. The idea of design can change the angle of the blades when the speed of the impeller increases, suitable for variable speed motors. Aiki et al. [13] presented in the patent a flexible blade fan that has a flexible tail section in each blade, which is constructed in one piece and is made of a synthetic resin material with a predetermined elasticity. This assembly is characterized by the fact that each blade is formed with the lead and trailing edges, reducing pitch angle as fan speed increases, reducing power requirements, and fan noise. Jackson et al. [14] showed a fan mechanism with flexible blades, and several elongated elements parallel to the longitudinal axis of the shaft for clamping the flexible belting roughly in the middle, resulting in two fan blades forming from each piece of belting. A retaining element located at either end of a plurality of extension members positions these members evenly around the circumference of the shaft. Cocks et al. [15] presented the flexible fan blade, which has a fixed middle section that is permanently attached to at least one of the centrifugal fan impeller's front plate and rear plate. Each flexible fan blade includes a fixed central portion and a portion that can be flexibly moved relative to the fixed center portion between a first position and a second position, multiple counterweights are attached to each movable part of the flexible fan.

In previous studies, the expansion of the effective operating area of the centrifugal fan has received much attention. This study develops a novel centrifugal fan with flexible blades that can change the inlet and outlet angle following different speeds. We have proposed a method to calculate the position of the propeller according to speed and mass flow. Based on the mathematical model, the study uses Matlab and Comsol Multiphysics to calculate the total rising pressure, efficiency, shaft torque, and shaft power of the fan in the case of the fixed and flexible blades at different speed ranges. Besides, an alternative to the standard $k - \epsilon$ model, the CFD by Comsol used the $k - \omega$ model which frequently provides more accurate findings, particularly in recirculation regions and adjacent to solid walls [16].

2. Methodology

The proposed flexible-blade centrifugal fan design is shown in Fig. 1. The blades can change position at different speeds and each blade is linked to two springs capable of rotating around the axis of rotation of each blade, the blades will rotate further forward as the angular speed of the impeller increases due to the springs are deformed. However, we also limit the change in position of the blades and ensure uniform displacement of the blades so the rotation angle of the blades is limited to the slide groove.

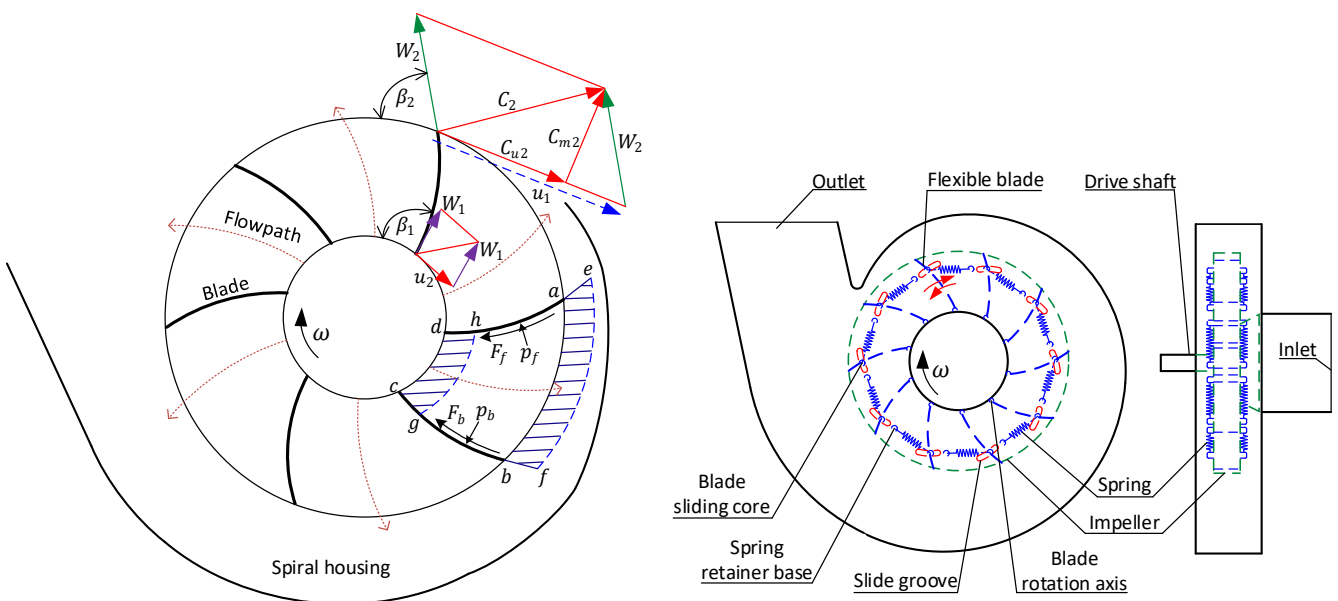
2.1. Theory of Centrifugal Fan

A rotating centrifugal impeller with backward blades is shown in Fig. 1. The fluid moves at the center of the impeller, impacted by the blades causing it to move at a right angle centrifugal outward thoroughly. The spiral housing collects the air to convert kinetic energy into static pressure and increases it. At any point along a flow path, the velocity may be expressed by vector components concerning either the rotating impeller or the fan spiral housing [1].

Figure 1 also presents the vector diagram for a particle of fluid leaving the impeller output. Where ω is the angular velocity of the impeller; u_1, u_2 are the inlet and outlet peripheral speed; C_{m1}, C_{m2} are the inlet and outlet radial components of fluid velocity, β_1, β_2 are the inlet and outlet vane angle; p_f, p_b are the pressure on the front of and on back of blade; F_f, F_b are the shear resistance on front of and on back of blade; C_1, C_2 are the inlet and outlet absolute fluid velocity; W_1, W_2 are the velocity tangential to the blade at the inlet and the outlet; C_{u1}, C_{u2} are the inlet and outlet peripheral component of fluid velocity.

Research by McPherson [1] pointed out that a torque, T , is maintained that is equal to the equivalent continuous rate of change of momentum if the mass flow is continuously being replaced (Euler's equation):

$$T = Q\rho[r_2C_{u2} - r_1C_{u1}] \tag{1}$$



(a) Diagram of velocities, forces on a centrifugal impeller [1] (b) Schematic configuration of fan with flexible blades

Fig. 1. Diagram of velocities, forces on a centrifugal impeller, and schematic configuration of fan with flexible blades.



where Q is the volume flow, ρ is the fluid density, r_1 is the inner radius of the impeller, r_2 is the outer radius of the impeller. The power consumed by the impeller can be written by the following equation [1]:

$$P_{ipl} = Q\rho[u_2C_{u2} - u_1C_{u1}] \quad (2)$$

In the case of ignoring friction or shock losses, the total pressure rise on the fan can be given by the following equation [1]:

$$p_{it} = \rho[u_2C_{u2} - u_1C_{u1}] \quad (3)$$

The inlet blade angle of the impeller [1]:

$$\tan \beta_1 = \frac{C_{m1}}{u_1 - C_{u1}} \quad (4)$$

The outlet blade angle of the impeller [1]:

$$\tan \beta_2 = \frac{C_{m2}}{u_2 - C_{u2}} \quad (5)$$

The inlet radial components of fluid velocity [17][18]:

$$C_{m1} = \frac{Q}{b[\pi D_1 - z\delta]} \quad (6)$$

The outlet radial components of fluid velocity [17][18]:

$$C_{m2} = \frac{Q}{b[\pi D_2 - z\delta]} \quad (7)$$

where b is the impeller width; D_1 , D_2 are the impeller inner and outer diameter, and δ is the thickness of the blade. From equations (3) to (7), the total pressure can be written:

$$p_{it} = \rho \left[u_2^2 - u_1^2 - \frac{u_2}{\tan \beta_2} \frac{Q}{b[\pi D_2 - z\delta]} + \frac{u_1}{\tan \beta_1} \frac{Q}{b[\pi D_1 - z\delta]} \right] \quad (8)$$

The overall efficiency of the centrifugal fan is [7]:

$$\eta_o = \frac{Qp_{it}}{P_s} = \frac{Qp_{it}}{\omega T_s} \quad (9)$$

where P_s is the shaft power input, T_s is the shaft torque input.

Selection of the number of blades with the backward-curved for $\beta_2 \leq 90^\circ$, following Pfleiderer yields [17]:

$$z = 5 \text{ to } 8 \left[\frac{1 + \frac{D_1}{D_2} \sin[0.5(\beta_1 + \beta_2)]}{1 - \frac{D_1}{D_2}} \right] \quad (10)$$

The principles of fluid flow, deal with the continuity equation and the energy balance equation. Those are the factors that need to be considered during the design of a centrifugal fan.

2.2. Kinematics of the Design Blade

Design blades can rotate to change the inlet and outlet angle of the airflow. In particular, a novelty in the blade adjustment system is that the blade (BC) moves around the center of rotation (C), the same for the remaining blades of the impeller. On the basis of the document [17], the geometric parameters of the blade are presented in Fig. 2.

The triangle (KBC) is constant when the blade angles (β_1, β_2) change. According to Autocad, the following relationship exists:

$$\beta_2 + \alpha = 75^\circ \quad (11)$$

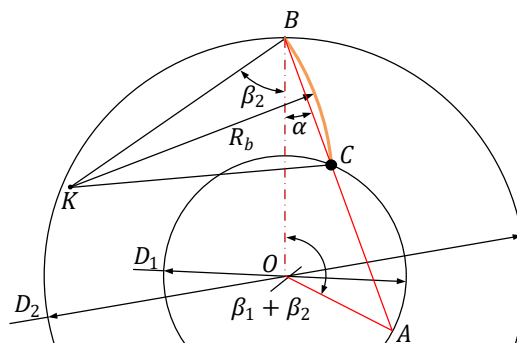


Fig. 2. Geometric parameters of the blade [17].



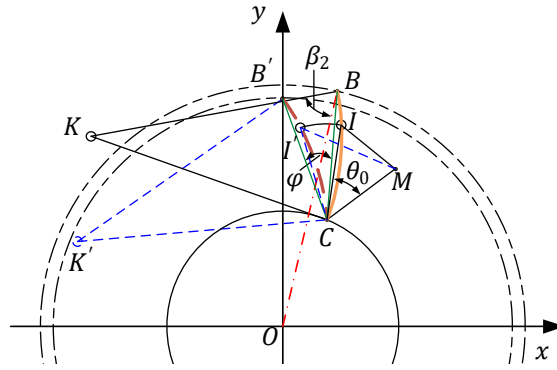


Fig. 3. Calculation diagram of design blade.

Consider triangle (OBA), the following equations can be obtained:

$$BA = \sqrt{OB^2 + OA^2 - 2OB \cdot OA \cdot \cos(\beta_1 + \beta_2)} \tag{12}$$

$$\frac{BA}{\sin(\beta_1 + \beta_2)} = \frac{OA}{\sin \alpha} \tag{13}$$

From equations (11) to (13), one can find the following expression:

$$\sin(75 - \beta_2) \sqrt{\frac{D_2^2}{4} + \frac{D_1^2}{4} - \frac{D_1 \cdot D_2}{2} \cos(\beta_1 + \beta_2)} = \frac{D_1}{2} \sin(\beta_1 + \beta_2) \tag{14}$$

To determine the coordinates of the points $B(x'_B, y'_B)$, $K(x'_K, y'_K)$ when (BC) rotates around the center $C(x_r, y_r)$, firstly, apply the translation $T(-x_r, -y_r)$ to move the center rotary back to the origin. Secondly, apply rotation $R(\varphi)$ to rotate (BC) around the origin with an angle φ . Finally, apply translation $T(x_r, y_r)$ to move the center of rotation from the origin to the original position.

Matrix equations where rotation is represented by multiplication and translation, is represented by addition. With homogeneous coordinates, we represent the coordinates of a point (x, y) in the form $(x/h, y/h, h)$. For convenience, we will choose $h = 1$, the matrix of geometric transformations is given as follows [19]:

$$R(x_r, y_r, \varphi) = T(x_r, y_r) \cdot R(\varphi) \cdot T(-x_r, -y_r) = \begin{bmatrix} 1 & 0 & x_r \\ 0 & 1 & y_r \\ 0 & 0 & 1 \end{bmatrix} \begin{bmatrix} \cos \varphi & -\sin \varphi & 0 \\ \sin \varphi & \cos \varphi & 0 \\ 0 & 0 & 1 \end{bmatrix} \begin{bmatrix} 1 & 0 & -x_r \\ 0 & 1 & -y_r \\ 0 & 0 & 1 \end{bmatrix} = \begin{bmatrix} \cos \varphi & -\sin \varphi & x_r(1 - \cos \varphi) + y_r \sin \varphi \\ \sin \varphi & \cos \varphi & y_r(1 - \cos \varphi) - x_r \sin \varphi \\ 0 & 0 & 1 \end{bmatrix} \tag{15}$$

The coordinates of initial points $B(x_B, y_B)$, $I(x_I, y_I)$, $K(x_K, y_K)$ and fixed point $M(x_M, y_M)$ are determined by Autocad. The coordinates of the points after performing the rotation of an angle φ are determined as follows:

The coordinates of the point $B(x'_B, y'_B)$:

$$B' = \begin{bmatrix} x'_B \\ y'_B \\ 1 \end{bmatrix} = R(x_r, y_r, \varphi) \cdot \begin{bmatrix} x_B \\ y_B \\ 1 \end{bmatrix} \tag{16}$$

$$B' = \begin{bmatrix} \cos \varphi & -\sin \varphi & x_r(1 - \cos \varphi) + y_r \sin \varphi \\ \sin \varphi & \cos \varphi & y_r(1 - \cos \varphi) - x_r \sin \varphi \\ 0 & 0 & 1 \end{bmatrix} \cdot \begin{bmatrix} x_B \\ y_B \\ 1 \end{bmatrix} \tag{17}$$

The coordinates of the point $K(x'_K, y'_K)$:

$$K' = \begin{bmatrix} x'_K \\ y'_K \\ 1 \end{bmatrix} = R(x_r, y_r, \varphi) \cdot \begin{bmatrix} x_K \\ y_K \\ 1 \end{bmatrix} \tag{18}$$

$$K' = \begin{bmatrix} \cos \varphi & -\sin \varphi & x_r(1 - \cos \varphi) + y_r \sin \varphi \\ \sin \varphi & \cos \varphi & y_r(1 - \cos \varphi) - x_r \sin \varphi \\ 0 & 0 & 1 \end{bmatrix} \cdot \begin{bmatrix} x_K \\ y_K \\ 1 \end{bmatrix} \tag{19}$$

The coordinates of the point $I(x'_I, y'_I)$:

$$I' = \begin{bmatrix} x'_I \\ y'_I \\ 1 \end{bmatrix} = R(x_r, y_r, \varphi) \cdot \begin{bmatrix} x_I \\ y_I \\ 1 \end{bmatrix} \tag{20}$$



$$I' = \begin{bmatrix} \cos \varphi & -\sin \varphi & x_r(1 - \cos \varphi) + y_r \sin \varphi \\ \sin \varphi & \cos \varphi & y_r(1 - \cos \varphi) - x_r \sin \varphi \\ 0 & 0 & 1 \end{bmatrix} \begin{bmatrix} x_i \\ y_i \\ 1 \end{bmatrix} \quad (21)$$

From the equations (17), (19) and (21), we have the following vectors:

$$\overrightarrow{BK} = \begin{bmatrix} \cos \varphi & -\sin \varphi & x_r(1 - \cos \varphi) + y_r \sin \varphi \\ \sin \varphi & \cos \varphi & y_r(1 - \cos \varphi) - x_r \sin \varphi \\ 0 & 0 & 1 \end{bmatrix} \begin{bmatrix} x_K - x_B \\ y_K - y_B \\ 0 \end{bmatrix} \quad (22)$$

$$\overrightarrow{BO} = \begin{bmatrix} \cos \varphi & -\sin \varphi & x_r(1 - \cos \varphi) + y_r \sin \varphi \\ \sin \varphi & \cos \varphi & y_r(1 - \cos \varphi) - x_r \sin \varphi \\ 0 & 0 & 1 \end{bmatrix} \begin{bmatrix} -x_B \\ -y_B \\ -1 \end{bmatrix} \quad (23)$$

$$\overrightarrow{MI} = \begin{bmatrix} \cos \varphi & -\sin \varphi & x_r(1 - \cos \varphi) + y_r \sin \varphi \\ \sin \varphi & \cos \varphi & y_r(1 - \cos \varphi) - x_r \sin \varphi \\ 0 & 0 & 1 \end{bmatrix} \begin{bmatrix} x_i \\ y_i \\ 1 \end{bmatrix} - \begin{bmatrix} x_M \\ y_M \\ 1 \end{bmatrix} \quad (24)$$

The vector \overrightarrow{MI} in equation (24) can be determined by the length $|\overrightarrow{MI}|$ when the blade (BC) rotates at an angle φ . The angle β_2 can be determined when the blade (BC) rotates at an angle φ :

$$\cos \beta_2 = \frac{\overrightarrow{BK} \cdot \overrightarrow{BO}}{|\overrightarrow{BK}| \cdot |\overrightarrow{BO}|} \quad (25)$$

Moczko et al. [2] and Ding et al. [4] used a model of a centrifugal fan with the following specifications are shown in Table 1.

According to the technical documents [20][21], the centrifugal fan for road sweepers has the main specifications presented in Table 2.

Based on fan specifications given by previous studies in Table 1 and the specifications of the fan for the road sweeper given by the technical documents in Table 2, design of fan input parameters such as airflow volume, speed, impeller diameter, etc are given in Table 3.

Table 1. The major design parameters.

Parameter	Moczko et al. [2]	Ding et al. [4]
Air flow volume (Q)	10000 m ³ /h	6200 m ³ /h
Total pressure (p _t)	2500 Pa	2700 Pa
Shaft Power (P _s)	---	30 kW
Speed (ω)	1500 rpm	1490 rpm
Temperature	---	25°C
Number of blades (Z)	12	16
Impeller inner diameter (D ₁)	---	368 mm
Impeller outer diameter (D ₂)	729 - 891 mm	810 mm
Impeller width (b)	121-122 mm	43 mm
Blades radius (R _b)	362 mm	---
Inlet blade angle (β ₁)	---	---
Outlet blade angle (β ₂)	---	29,5°

Table 2. The parameters of a fan for road sweepers.

Parameter	Merlin XP Hydrostatic [20]	Global R3 Air [21]
Air flow volume (Q)	10200 m ³ /h	---
Number of blades (Z)	---	9
Impeller outer diameter (D ₂)	905,5 mm	838,2 mm
Speed Standard	2000 rpm	2450 rpm
Speed Boost	2200 rpm	---



Table 3. The input parameters of the designed centrifugal fan.

Parameter	Value
Air flow volume (Q)	7000 - 22000 m ³ /h
Speed (ω)	1500 - 3500 rpm
Temperature	40°C
Fluid density (ρ)	1,127 kg/m ³
Impeller inner diameter (D ₁)	395 mm
Impeller outer diameter (D ₂)	781,1 - 827,4 mm
Impeller width (b)	85 mm
Blades radius (R _b)	427,5 mm
Inlet blade angle (β ₁)	62,64° - 87,16°
Outlet blade angle (β ₂)	55,08° - 66,59°
Rotation blade angle (φ)	0°-24,6°

2.3. Dynamics of the Design Blade

The flexible blade in Fig. 4 is designed to change blade angles with speed and air resistance. Where k_s is spring stiffness, F is spring force, Δl is the deformation of the spring so that the spring force at the initial position is equal to the inertia force due to the flow through the blade:

$$F_{lx} = k_s \cdot (|\vec{I'M}| - |\vec{IM}| + \Delta l) \tag{26}$$

Application of Newton’s second law for rotation of the blade (BC) in Fig. 4, yields:

$$F_{lx} \cdot d_1 = \frac{Q \cdot p_{tt}}{\omega} + I_{BC} \cdot \varphi'' \tag{27}$$

or

$$F_{lx} \cdot d_1 = \frac{Q}{\omega} \cdot \rho \left[u_2^2 - u_1^2 - \frac{u_2}{\tan \beta_2} \frac{Q}{b[\pi D_2 - z \cdot \delta]} + \frac{u_1}{\tan \beta_1} \frac{Q}{b[\pi D_1 - z \cdot \delta]} \right] + I_{BC} \cdot \varphi'' \tag{28}$$

where F_{lx} is spring force, I_{BC} is the moment of inertia of the blade (BC) with respect to the center of rotation C, d_1 is the perpendicular distance of spring force which can be given as equation:

$$d_1 = \frac{I'_{C.MC} \cdot \sin(\theta_0 + \varphi)}{I'M} \tag{29}$$

From equation (28), equation (29) can calculate spring stiffness (k_s) with the following conditions:

- The first condition: the speed of the impeller is 1500 rpm, rotation blade angle $\varphi = 0^\circ$, $|\vec{M'I}| = \min$.
- The second condition: the speed of the impeller is 3500 rpm, rotation blade angle $\varphi = 24,6^\circ$, $|\vec{M'I}| = \max$.

2.4. Design of Centrifugal Fan

Figure 5(a) shows the assemblies or components of a flexible fan including fan inlet flange, fan cover plate 1, fan outlet flange, fan housing, fan cover plate 2, and fan impeller. Figure 5(b) presents the separation assemblies of the fan impeller including impeller flange 1, blades, impeller flange 2, the slip track of blades and spring hook point, nut M18, spring, and fluid flow direction pipe. The proposed flexible fan is designed using Solidworks as input data for CFD simulation by Comsol Multiphysics and statistical calculations by Matlab.

In Fig. 5, the calculation diagram of a flexible propeller is presented with the input parameters as blade design parameters (Q, ρ), impeller parameters (D₁, D_{2min}, D_{2max}, b, δ, z), and type of casing. Besides, estimate the speed range and blade angle range to calculate spring stiffness for flexible blades. For each rotation angle of the blade, we will calculate the speed and angles blade (β_{1i}, β_{2i}). Figure 6 presents the flow chart of the current design algorithm.

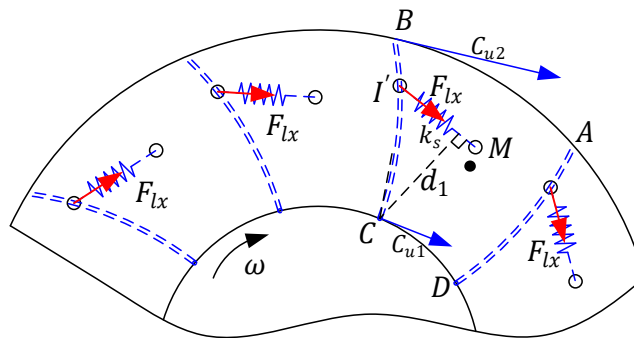
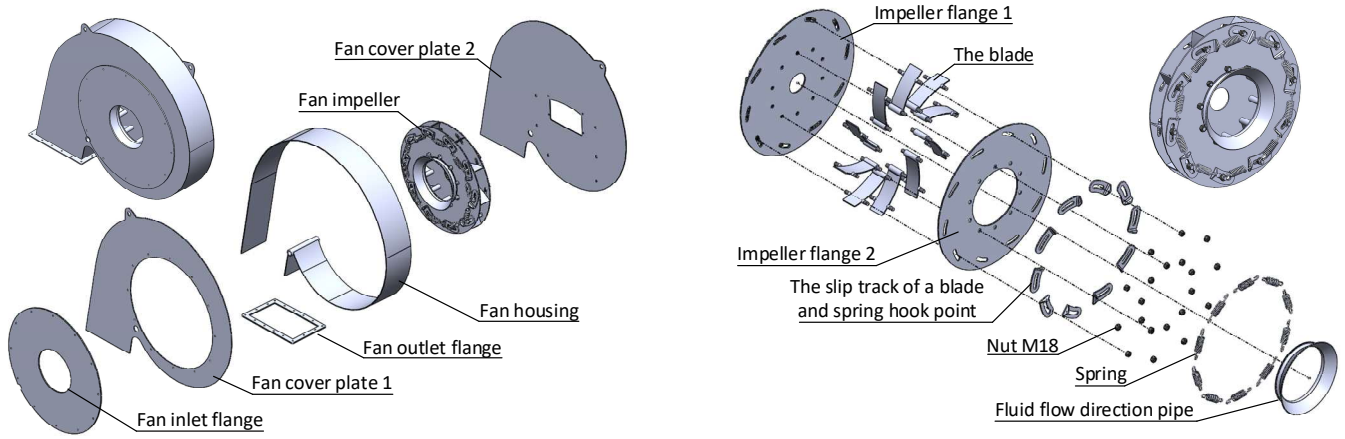


Fig. 4. Dynamic diagram of design blade.





(a) Separation assemblies of centrifugal fan

(b) Separation assemblies of fan impeller

Fig. 5. 3D model of the design of centrifugal impeller with the flexible backward-bladed.

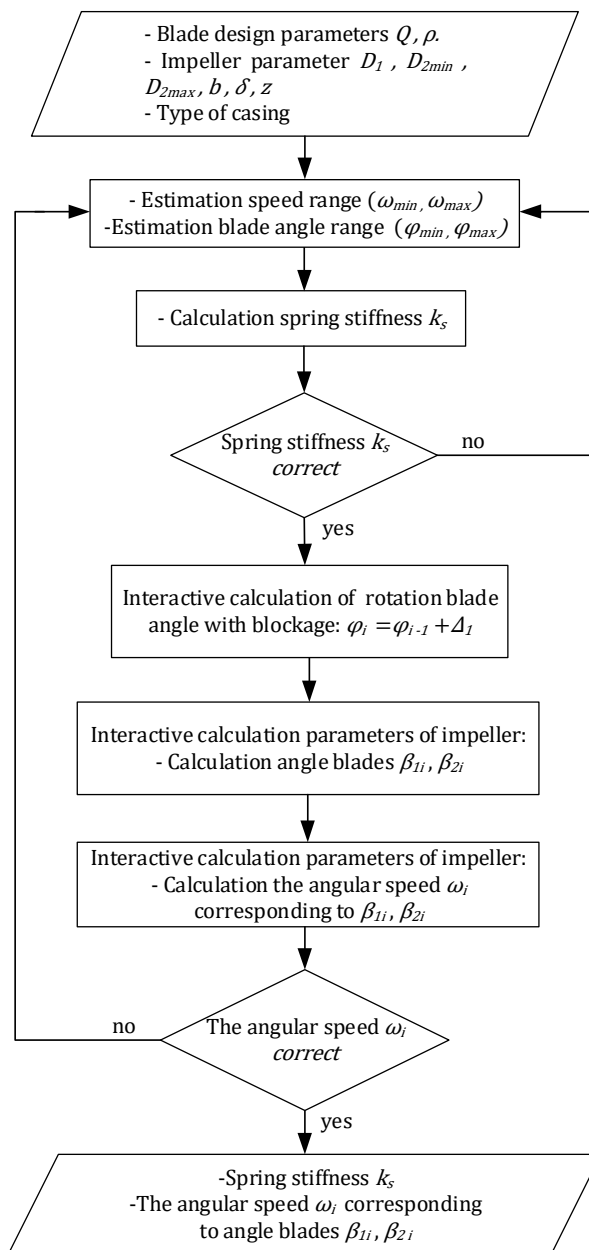


Fig. 6. Flow chart: Design of centrifugal impeller with the flexible backward-bladed.



Table 4. The parameters of the simulation model.

Parameter	Value
Fluid density (ρ)	1,127 kg/m ³
Temperature	40°C
Air flow volume (Q)	7000 - 22000 m ³ /h
Speed (ω)	1500 - 3500 rpm
Inlet diameter	∅360 mm
Outlet size	432x230 mm

Table 5. Analysis of mesh sensitivity to centrifugal fan models.

Models	Speed (rpm)	Maximum element size	Minimum element size	Number of elements	Average element quality	Minimum element quality	Total rise pressure (Pa)	Error (%)
Fixed Blade 1 Flexible Blade	1500	0,065	0,013	320637	0,6617	0,1893	2419,0	7,083
		0,055	0,011	433030	0,6629	0,2207	2506,3	3,730
		0,0487	0,00919	637430	0,6628	0,1802	2620,2	0,645
		0,02	0,0065	1196791	0,6628	0,215	2603,4	0,000
Fixed Blade 1	3500	0,065	0,013	320644	0,6617	0,1893	8947,7	15,212
		0,055	0,011	433036	0,6629	0,2207	9610,5	8,931
		0,0487	0,00919	637430	0,6628	0,1802	10533,0	0,190
		0,02	0,0065	1196803	0,6628	0,215	10553,0	0,000
Fixed Blade 2	1500	0,065	0,013	312391	0,66	0,1702	1738,8	8,436
		0,055	0,011	417372	0,6623	0,1637	1804,2	4,992
		0,0487	0,00919	607501	0,6613	0,1501	1889,0	0,537
		0,02	0,0065	1162401	0,6624	0,2013	1899,2	0,000
Fixed Blade 2 Flexible Blade	3500	0,065	0,013	312391	0,66	0,1702	4787,5	13,525
		0,055	0,011	417372	0,6623	0,1637	5158,6	6,822
		0,0487	0,00919	607501	0,6613	0,1501	5708,1	3,103
		0,02	0,0065	1162401	0,6624	0,2013	5536,3	0,000

2.5. CFD model

Table 4 presents the input parameters used for CFD simulation of the centrifugal fan including parameters such as fluid density, temperature, airflow volume, speed, inlet diameter, and outlet size. Output parameters to be found using CFD include pressure rise, power, and fan efficiency.

The rising pressure, power, and efficiency of flexible fans are explored using CFD simulations on the Comsol Multiphysics software with $k-\omega$ model. This study used a simulation model that includes inlet air block, spiral housing air block, impeller air block, and outlet air block in Fig. 7.

The 3D model of the centrifugal fan with geometric parameters as shown in Fig. 7(a) is converted to a mesh model to conduct CFD simulation as shown in Fig. 7(b). A free tetrahedral mesh was used for the centrifugal fan model (Fig. 7(b)). The element quality is a number between 0 and 1, where 0 denotes a fully flat or degenerated element and 1 defines an element that is perfectly symmetric. A minimal quality of roughly 0.1 indicates a good mesh for 3D meshes in general [22].

Thong et al. [23] presented a numerical validation method using a mesh-independent test. By a similar method presented in Table 5, an independent test of the mesh was performed to ensure the accuracy of the numerical simulation result. The value of total rise pressure corresponding to the number of mesh elements is shown in Table 5 for centrifugal fan models at 1500 rpm and 3500 rpm. Considering the models at six hundred thousand elements and one million one hundred thousand elements, the error of total rise pressure for the models Fixed Blade 2 and Flexible Blade at 3500 rpm is 3,103%, and the errors for all other cases are less than 0.645%. We can see that this difference is insignificant and completely acceptable. So, the six hundred thousand elements grid was chosen to create a balance between the computational resources and the quality of the simulation results. The mesh parameters are shown in Table 6.

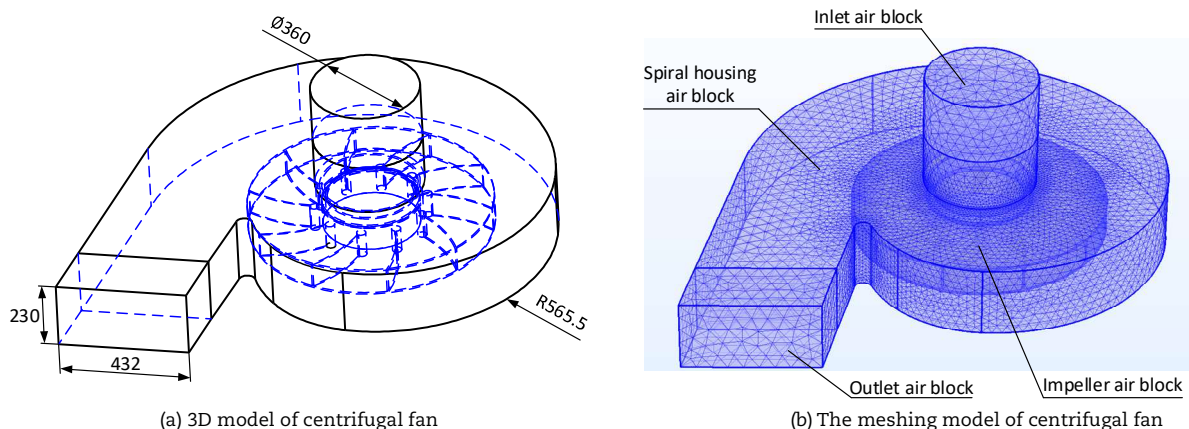
**Fig. 7.** 3D model and the meshing model of centrifugal fan.

Table 6. The grid parameters and turbulence model.

Parameter	Value/ Type
Maximum element size (Grid)	0,0487 m
Minimum element size (Grid)	0,00919 m
Turbulence model type	RANS
Turbulence model	$k - \omega$

Table 6 describes the parameters of the computational grid including the maximum element size and minimum element size. The turbulence model type used for this investigation is the Reynolds-Averaged Navier-Stokes (RANS) with $k - \omega$ model. The continuity, and the momentum equation are described as follows [16]:

$$\rho \nabla \cdot \mathbf{u} = 0 \quad (30)$$

$$\rho \frac{\partial \mathbf{u}}{\partial t} + \rho (\mathbf{u} \cdot \nabla) \mathbf{u} = \nabla \cdot [-p\mathbf{I} + (\mu + \mu_T)(\nabla \mathbf{u} + (\nabla \mathbf{u})^T)] + \mathbf{F} \quad (31)$$

In the $k - \omega$ model, the dissipation per unit of turbulent kinetic energy is ω and the turbulent kinetic energy is defined by k . The CFD equations of this model are shown below [16]:

$$\rho \frac{\partial k}{\partial t} + \rho \mathbf{u} \cdot \nabla k = P_k - \rho \beta^* k \omega + \nabla \cdot ((\mu + \mu_T \sigma^*) \nabla k) \quad (32)$$

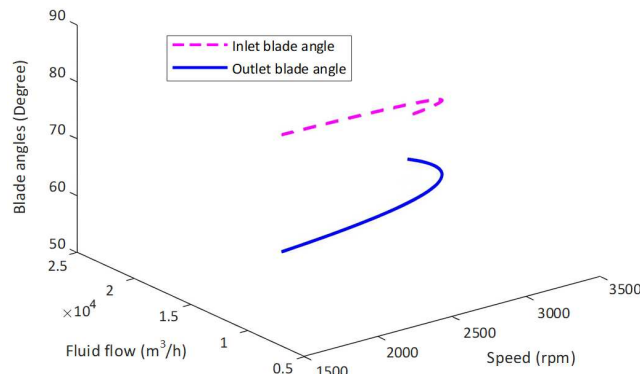
$$\rho \frac{\partial \omega}{\partial t} + \rho \mathbf{u} \cdot \nabla \omega = \alpha \frac{\omega}{k} P_k - \rho \beta \omega^2 + \nabla \cdot ((\mu + \mu_T \sigma) \nabla \omega) \quad (33)$$

The turbulent viscosity is calculated by:

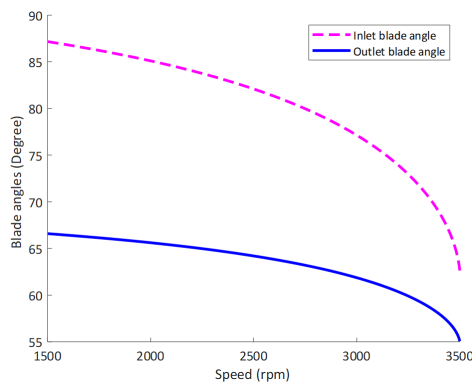
$$\mu_T = \rho \frac{k}{\omega} \quad (34)$$

where \mathbf{u} , μ , \mathbf{F} are the velocity vector, the dynamic viscosity and the volume force vector, respectively. Detailed descriptions of P_k , β^* , σ^* , β can be found in Ref. [16].

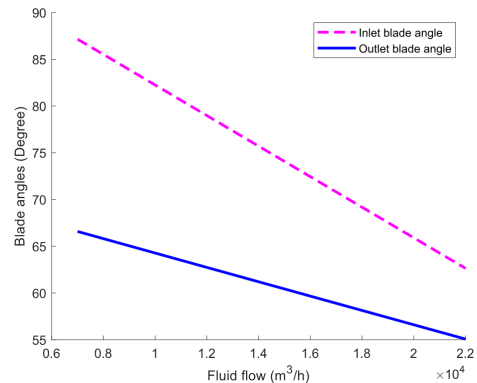
In addition, the convergence criterion of the nonlinear model calculation is set to be 10^{-6} (0.0001% relative error/tolerance). The numerical solution satisfies the numerical convergence criteria when the relative tolerance is 0.1%.



(a) The blade angles according to speed and fluid flow



(b) The blade angles according to speed



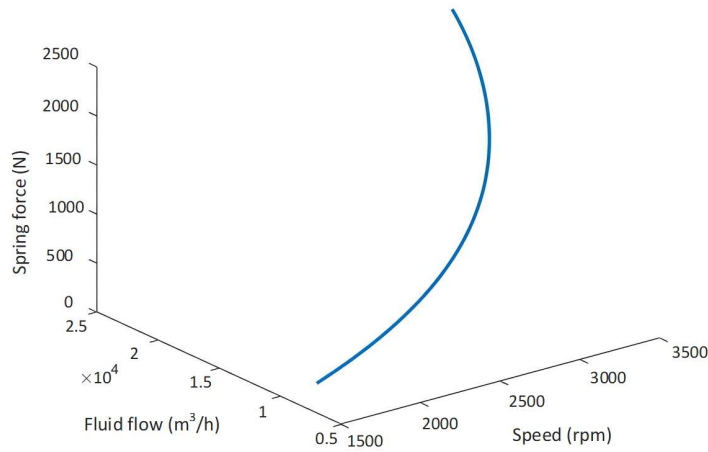
(c) The blade angles according to fluid flow

Fig. 8. The blade angles according to speed and fluid flow.

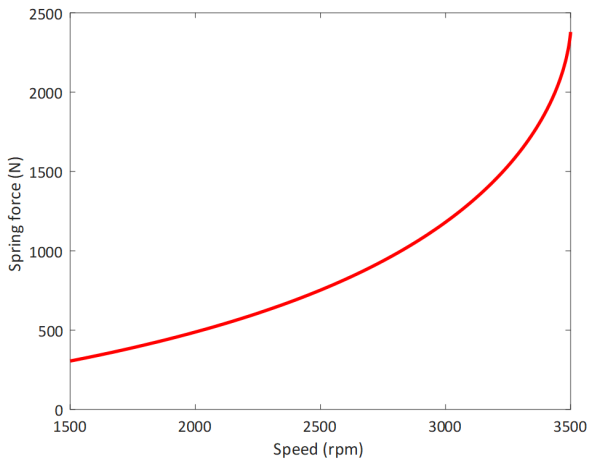

3. Results

Figure 8(a) shows the change of blade angles according to speed and fluid flow. Figure 8(b) shows that for the speed region below 2500 rpm, where the blade angle changes are almost linear. But for the speed region from 2500-3500 rpm, the blade angle changes are nonlinear curves. Figure 8(c) shows the change of blade angles when the fluid flow is assumed to be linear. When the blades are in the initial position, one has $\beta_1 = 87,16^\circ$, $\beta_2 = 66,59^\circ$, and for the blades in the last position, one obtains $\beta_1 = 62,64^\circ$, $\beta_2 = 55,09^\circ$.

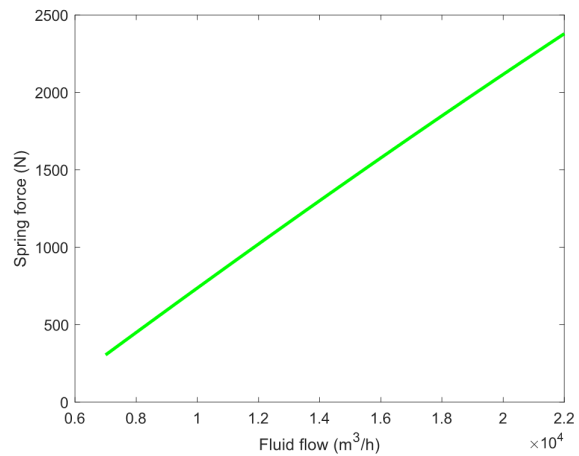
Figure 9(a) shows the change in spring force of flexible blades according to speed and fluid flow. The change in spring force of the flexible blade is non-linear with speed. For the high-speed region above 2500 rpm, the spring force changes a lot and is non-linear in Fig. 9(b). The change of the spring force according to fluid flow is linear.



(a) The spring force according to speed and fluid flow

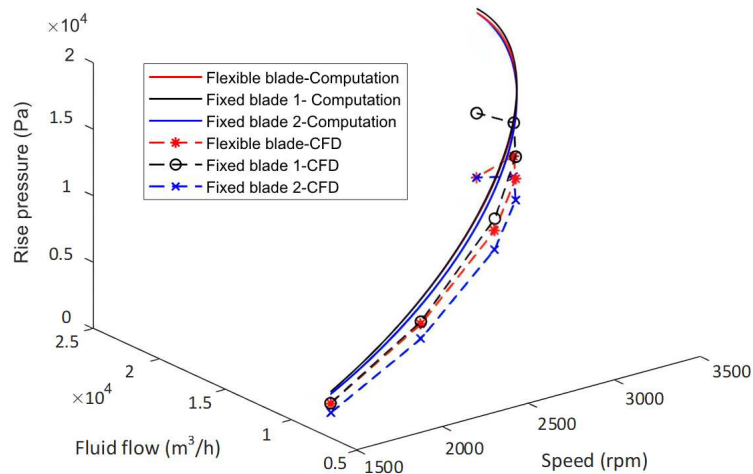


(b) The spring force according to speed



(c) The spring force according to fluid flow

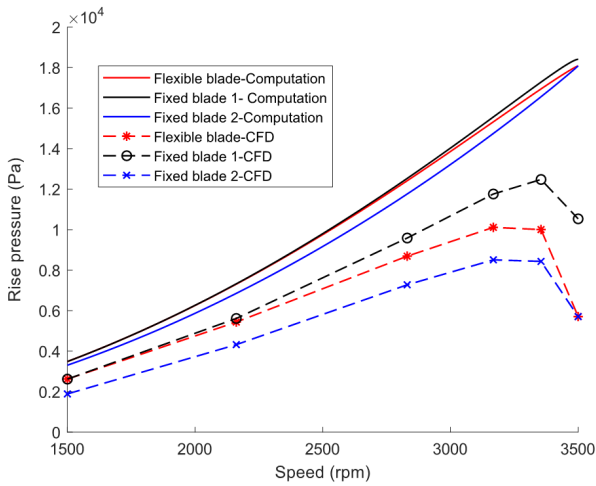
Fig. 9. The spring force of the fan blade.



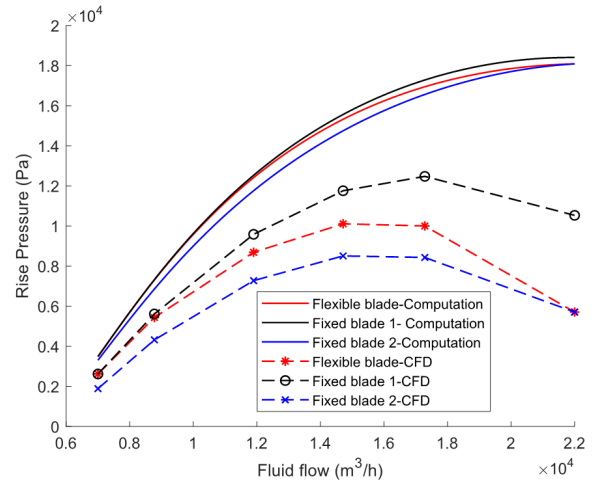
(a) The rising pressure according to speed and fluid flow

Fig. 10. The rising pressure of the centrifugal fan.



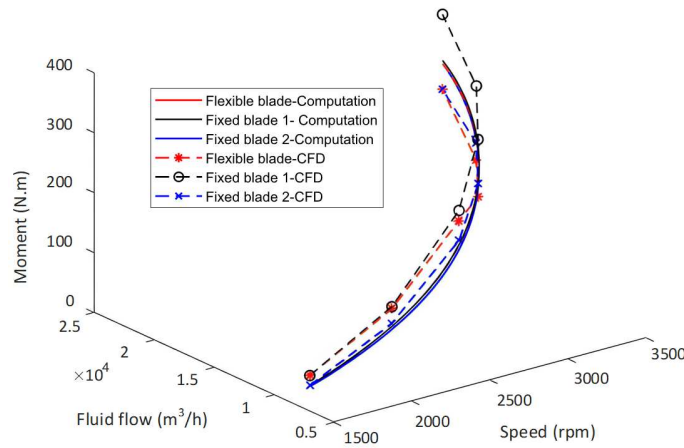


(b) The rising pressure according to speed

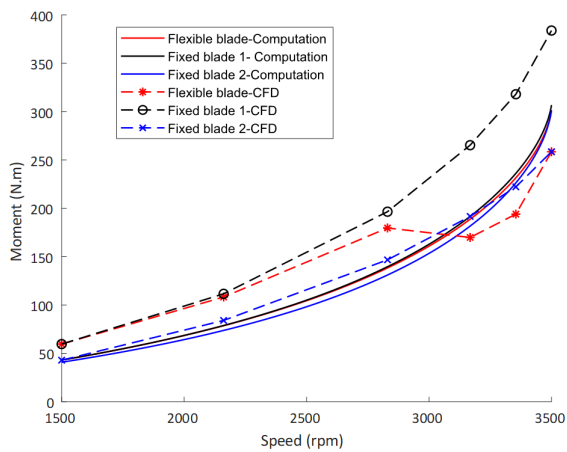


(c) The rising pressure according to fluid flow

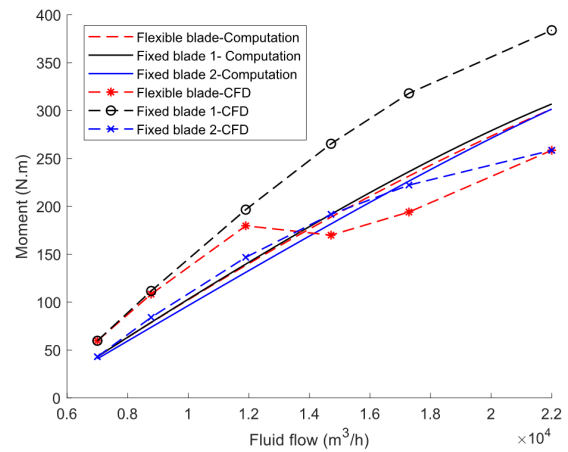
Fig. 10. Continued.



(a) The moment of the impeller according to speed and fluid flow



(b) The moment of the impeller according to speed



(c) The moment of the impeller according to fluid flow

Fig. 11. The moment of the fan impeller.

Figure 10 shows the rising pressure of a flexible fan and two other types of fixed blades. Figure 10(a) describes the change of the rising pressure of the flexible fan according to speed and fluid flow, Figs. 10(b) and 10(c) show that the rising pressure of the considered fans increases steadily for the speed range from 1500-3167 rpm and for the fluid flow range from 7000-14714 m^3/h , the rising pressure tends to decrease with the speed range from 3167-3500 rpm and flow range from 14714-22000 m^3/h .

Figures 11 and 12 show the moment and the power consumption of the impeller according to speed and fluid flow. Besides, Figs. 11 and 12 present that the power consumption and moment of the flexible fan are higher than Fixed blade 2 and smaller than fixed blade 1 in the speed range from 1500-3167,85 rpm and fluid flow range from 7000 to 14714,3 m^3/h . However, the flexible fan has lower power consumption and torque than fixed blade 1 and fixed blade 2 at high-speed range from 3167,85 to 3500 rpm fluid flow range from 14714,3 to 22000 m^3/h .



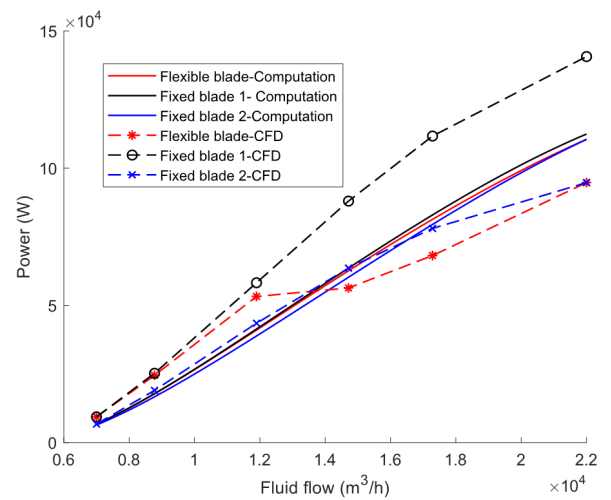
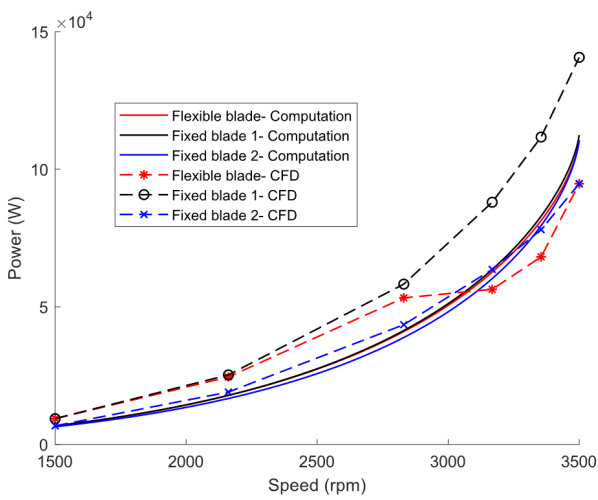
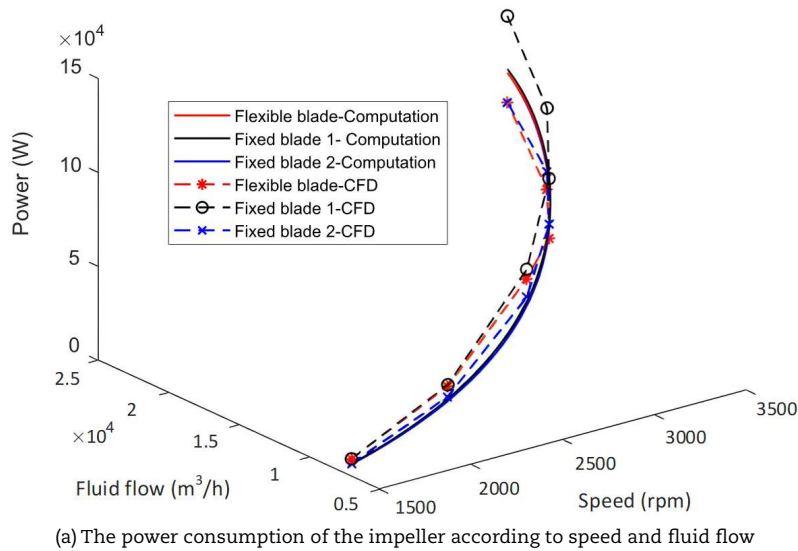


Fig. 12. The power consumption of the fan impeller.

Table 7. The results between CFD simulation and statistical computation at speed 1500 rpm and fluid flow 7000 m³/h.

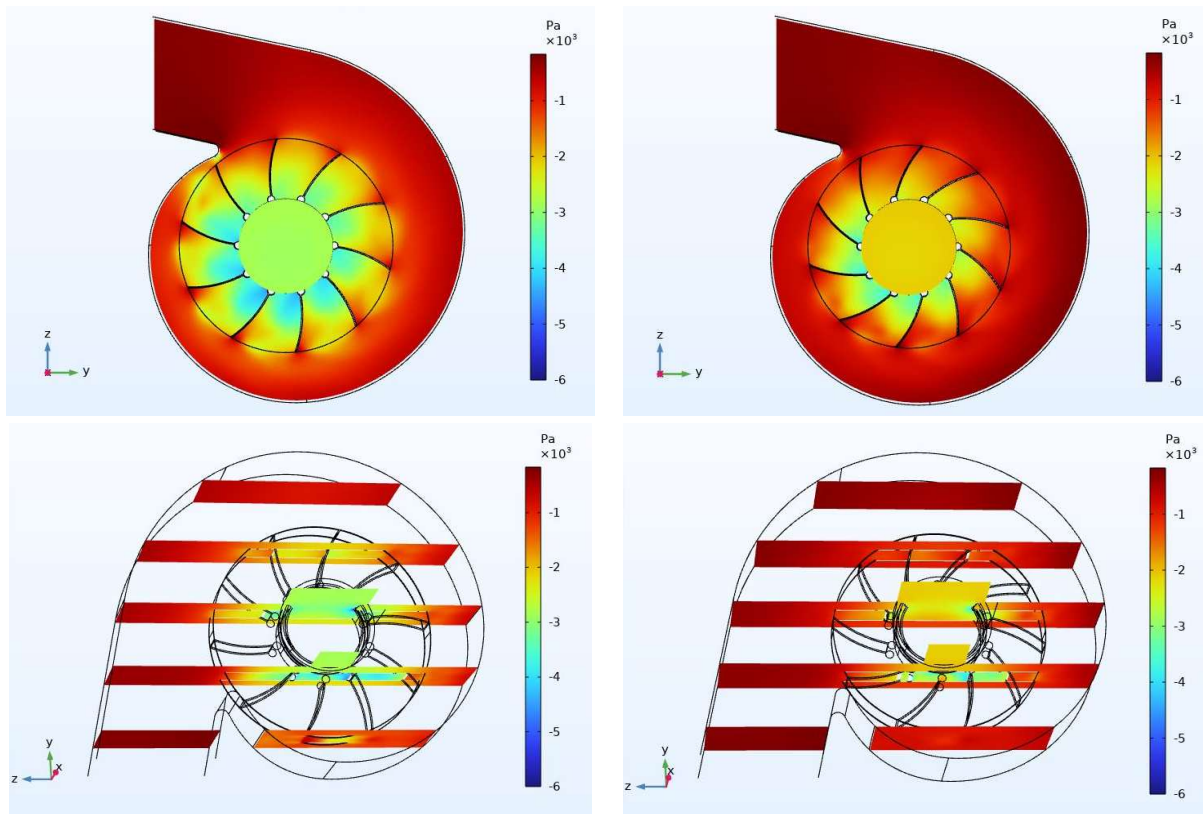
No.	Parameters	Fixed Blade 1	Fixed Blade 2	Flexible Blade
1	Impeller inner diameter (D_1), [mm]	395	395	395
2	Impeller outer diameter (D_2), [mm]	827,4	781,1	827,4
3	Speed (ω), [rpm]	1500	1500	1500
4	Air flow volume (Q), [m ³ /h]	7000	7000	7000
5	Inlet blade angle (β_1), [degree]	87,16	62,64	87,16
6	Outlet blade angle (β_2), [degree]	66,59	55,09	66,59
7	Total rise pressure computation (p_t), [Pa]	3488,18	3307,12	3488,18
8	Total rise pressure, CFD (p_t), [Pa]	2620,2	1889,0	2620,2
9	Error total rise pressure, [%]	24,88	42,88	24,88
10	Shaft Power, CFD (P_{shaft}), [kW]	9,377	6,759	9,377
11	Shaft Torque, CFD (T_{shaft}), [N.m]	59,695	43,032	59,695
12	Efficiency, CFD (η_s), [%]	54,33	54,34	54,33

Tables 6 to 9 present the parameters of the flexible blade for comparison with two other types of fixed blades: fixed blade 1 and fixed blade 2 for the speed range from 1500 to 3167,85 rpm and fluid flow from 7000 to 14714,3 m³/h. In particular, the flexible blade of the centrifugal fan at $\omega = 3167,85$ rpm and $Q = 14714,3$ m³/h has the lowest power consumption of 56,379 kW and the highest efficiency of 73,31%. Figures 13 to 16 present the total pressure contours with different speeds and flows with three models of the centrifugal fan. The pressure spectrum of the fan is shown on the plane passing through the impeller (oyz) and 5 planes perpendicular to the impeller (oxz).



Table 8. The results between CFD simulation and statistical computation at speed 2161,31 rpm and fluid flow 8775,51 m³/h.

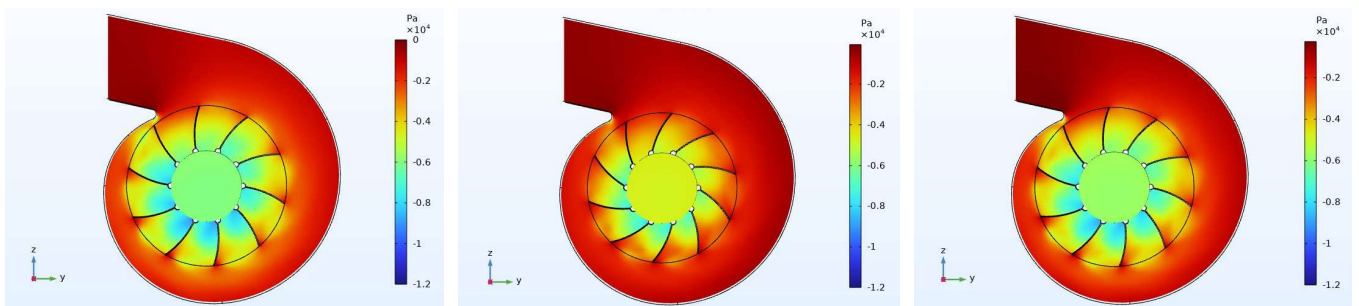
No.	Parameters	Fixed Blade 1	Fixed Blade 2	Flexible Blade
1	Impeller inner diameter (D_1), [mm]	395	395	395
2	Impeller outer diameter (D_2), [mm]	827,4	781,1	823,8
3	Speed (ω), [rpm]	2161,31	2161,31	2161,31
4	Air flow volume (Q), [m ³ /h]	8775,51	8775,51	8775,51
5	Inlet blade angle (β_1), [degree]	87,16	62,64	84,26
6	Outlet blade angle (β_2), [degree]	66,59	55,09	65,22
7	Total rise pressure computation (p_t), [Pa]	7325,51	6854,2	7309,39
8	Total rise pressure CFD (p_t), [Pa]	5614,7	4322,0	5437,2
9	Error total rise pressure, [%]	23,35	36,94	25,61
10	Shaft Power, CFD (P_{shaft}), [kW]	25,277	19,045	24,528
11	Shaft Torque, CFD (T_{shaft}), [N.m]	111,68	84,148	108,37
12	Efficiency, CFD (η_o), [%]	54,15	55,32	54,04



(a) Fixed Blade 1 and Flexible Blade

(b) Fixed Blade 2

Fig. 13. The rising pressure of the centrifugal fan using CFD simulation at $\omega = 1500$ rpm and $Q = 7000$ m³/h.



(a) Fixed Blade 1

(b) Fixed Blade 2

(c) Flexible Blade

Fig. 14. The rising pressure of the centrifugal fan using CFD simulation at $\omega = 2161,31$ rpm and $Q = 8775,51$ m³/h.



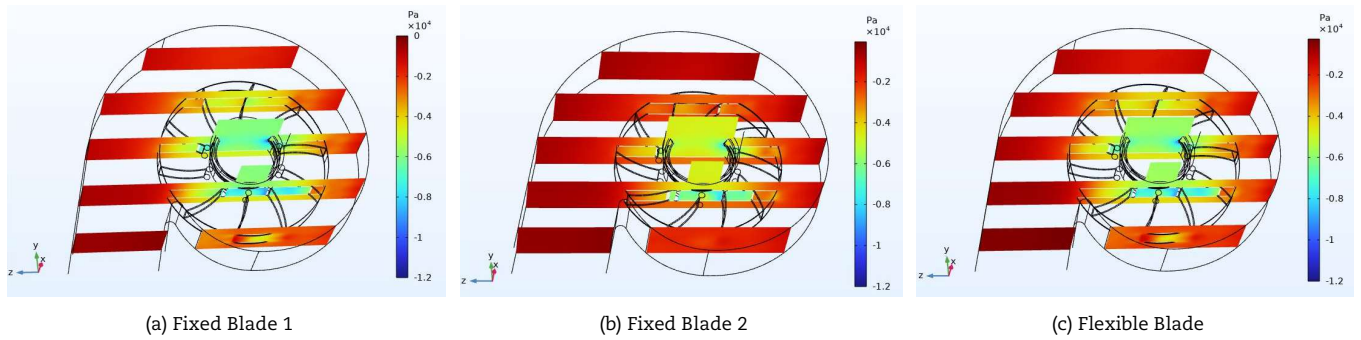


Fig. 14. Continued.

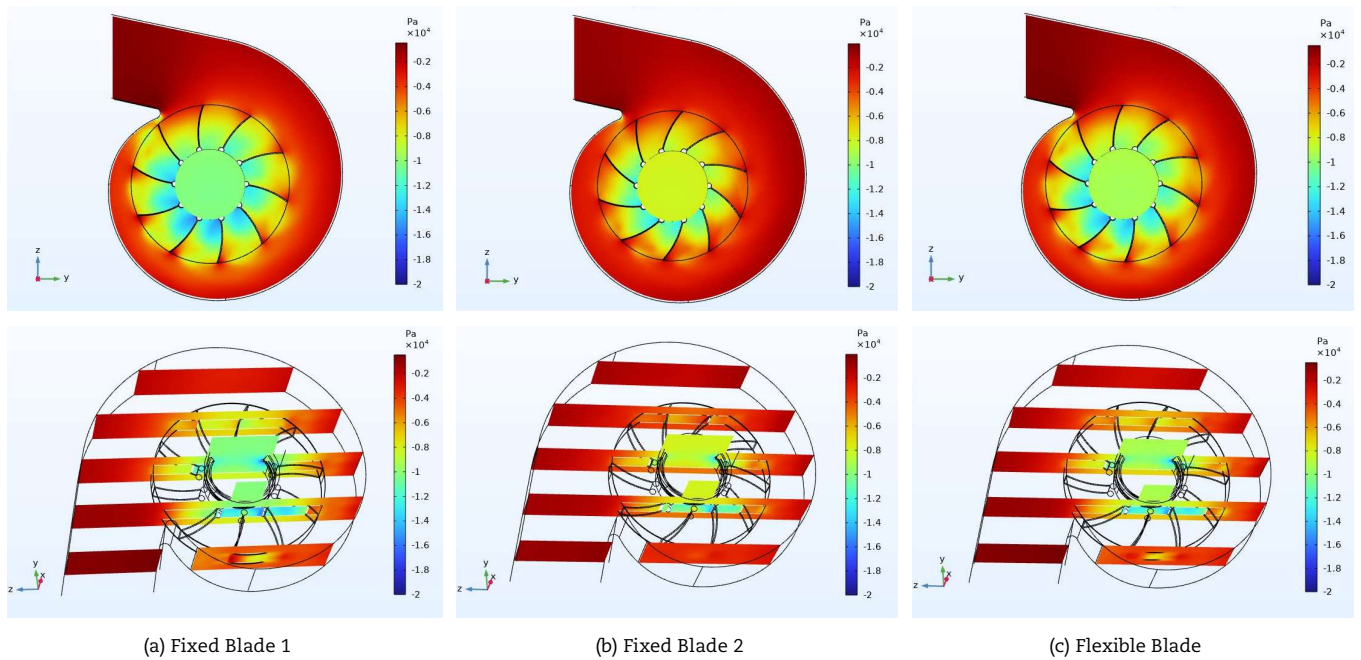


Fig. 15. The rising pressure of the centrifugal fan using CFD simulation at $\omega = 2830,51 \text{ rpm}$ and $Q = 11898 \text{ m}^3/\text{h}$.

Table 9. The results between CFD simulation and statistical computation at speed 2830,51 rpm and fluid flow 11898 m³/h.

No.	Parameters	Fixed Blade 1	Fixed Blade 2	Flexible Blade
1	Impeller inner diameter (D_1), [mm]	395	395	395
2	Impeller outer diameter (D_2), [mm]	827,4	781,1	813,4
3	Speed (ω), [rpm]	2830,51	2830,51	2830,51
4	Air flow volume (Q), [m^3/h]	11898	11898	11898
5	Inlet blade angle (β_1), [degree]	87,16	62,64	79,15
6	Outlet blade angle (β_2), [degree]	66,59	55,09	62,82
7	Total rise pressure computation (p_{tt}), [Pa]	12530,2	11760,5	12414,5
8	Total rise pressure, CFD (p_{tt}), [Pa]	9586,3	7276,5	8689,3
9	Error total rise pressure, [%]	23,49	38,13	30,01
10	Shaft Power, CFD (P_{shaft}), [kW]	58,274	43,525	53,28
11	Shaft Torque, CFD (T_{shaft}), [N.m]	196,60	146,84	179,75
12	Efficiency, CFD (η_o), [%]	54,37	55,25	53,90

The flexible blade of the centrifugal fan at $\omega = 3354,51 \text{ rpm}$ and $Q = 17285,7 \text{ m}^3/\text{h}$ has a power consumption of 68,181 kW and an efficiency of 70,45 %, compared with the other two types of blades at the same speed and flow conditions, flexible blades have lower power consumption but higher efficiency. Besides, Table 10 and Fig. 17 show that the rising pressure of a flexible fan is relatively high reaching 10003 Pa.



Table 10. The results between CFD simulation and statistical computation at speed 3167,85 rpm and fluid flow 14714,3 m³/h.

No.	Parameters	Fixed Blade 1	Fixed Blade 2	Flexible Blade
1	Impeller inner diameter (D_1), [mm]	395	395	395
2	Impeller outer diameter (D_2), [mm]	827,4	781,1	808,2
3	Speed (ω), [rpm]	3167,85	3167,85	3167,85
4	Air flow volume (Q), [m ³ /h]	14714,3	14714,3	14714,3
5	Inlet blade angle (β_1), [degree]	87,16	62,64	74,55
6	Outlet blade angle (β_2), [degree]	66,59	55,09	60,66
7	Total rise pressure computation (p_{tt}), [Pa]	15564,2	14749,3	15324,3
8	Total rise pressure, CFD (p_{tt}), [Pa]	11760	8509,2	10112,0
9	Error total rise pressure, [%]	24,44	42,31	34,01
10	Shaft Power, CFD (P_{shaft}), [kW]	88,036	63,604	56,379
11	Shaft Torque, CFD (T_{shaft}), [N.m]	265,38	191,73	169,95
12	Efficiency, CFD (η_a), [%]	54,60	54,68	73,31

Table 11. The results between CFD simulation and statistical computation at speed 3354,51 rpm and fluid flow 17285,7 m³/h.

No.	Parameters	Fixed Blade 1	Fixed Blade 2	Flexible Blade
13	Impeller inner diameter (D_1), [mm]	395	395	395
14	Impeller outer diameter (D_2), [mm]	827,4	781,1	799,6
15	Speed (ω), [rpm]	3354,51	3354,51	3354,51
16	Air flow volume (Q), [m ³ /h]	17285,7	17285,7	17285,7
17	Inlet blade angle (β_1), [degree]	87,16	62,64	70,35
18	Outlet blade angle (β_2), [degree]	66,59	55,09	58,69
19	Total rise pressure computation (p_{tt}), [Pa]	17283,5	16562,3	16947,2
20	Total rise pressure, CFD (p_{tt}), [Pa]	12477,0	8432,2	10003
21	Error total rise pressure, [%]	27,81	49,09	40,98
22	Shaft Power, CFD (P_{shaft}), [kW]	111,729	78,076	68,181
23	Shaft Torque, CFD (T_{shaft}), [N.m]	318,06	222,26	194,09
24	Efficiency, CFD (η_a), [%]	53,62	51,86	70,45

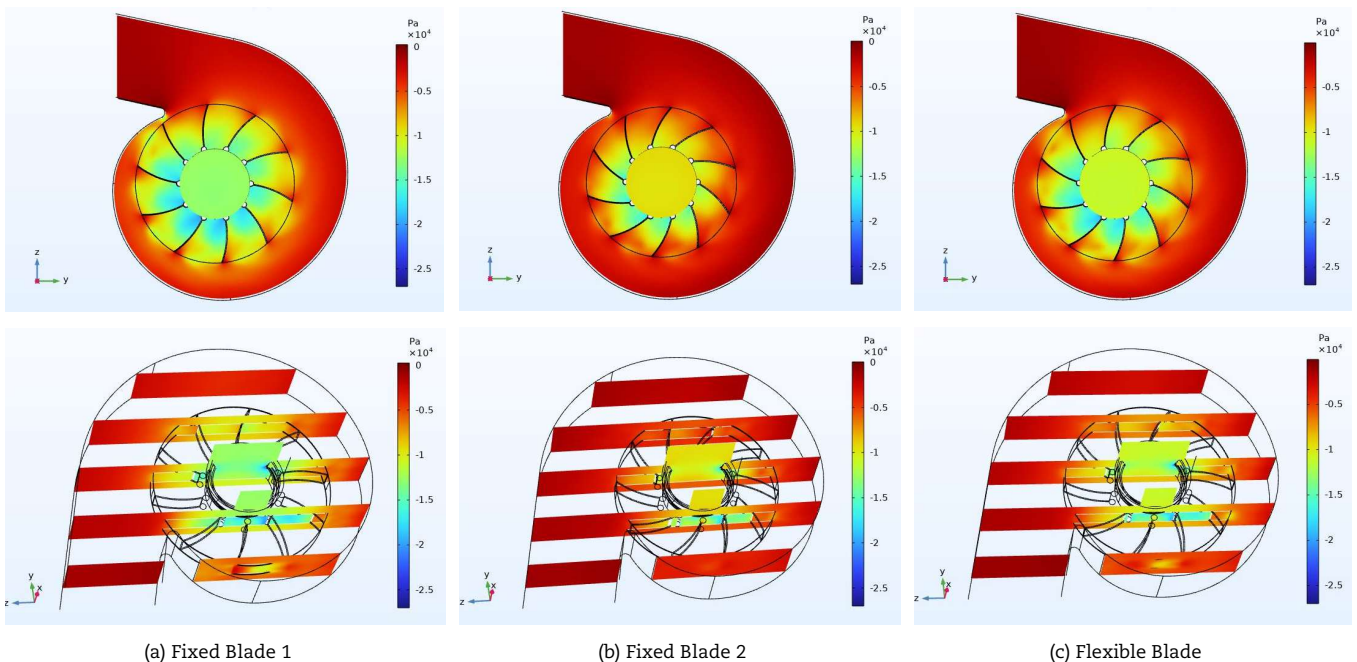
**Fig. 16.** The rising pressure of the centrifugal fan using CFD simulation at $\omega = 3167,85$ rpm and $Q = 14714,3$ m³/h.

Table 12. The results between CFD simulation and statistical computation at speed 3500 rpm and fluid flow 22000 m³/h.

No.	Parameters	Fixed Blade 1	Fixed Blade 2	Flexible Blade
1	Impeller inner diameter (D_1), [mm]	395	395	395
2	Impeller outer diameter (D_2), [mm]	827,4	781,1	781,1
3	Speed (ω), [rpm]	3500	3500	3500
4	Air flow volume (Q), [m ³ /h]	22000	22000	22000
5	Inlet blade angle (β_1), [degree]	87,16	62,64	62,64
6	Outlet blade angle (β_2), [degree]	66,59	55,09	55,09
7	Total rise pressure computation (p_{tt}), [Pa]	18405,7	18087,9	18087,9
8	Total rise pressure, CFD (p_{tt}), [Pa]	10533,0	5708,1	5708,1
9	Error total rise pressure, [%]	42,77	68,44	68,44
10	Shaft Power, CFD (P_{shaft}), [kW]	140,710	94,771	94,771
11	Shaft Torque, CFD (T_{shaft}), [N.m]	383,91	258,57	258,57
12	Efficiency, CFD (η_a), [%]	45,75	36,81	36,81

4. Conclusion

This paper presented a centrifugal fan with flexible blades that can change the blade's angle at different speeds and flow volume ranges. The goal of the study was to extend the effective range of the fan. When the fan operates at low speed and low flow volume, there is a high-pressure rise. When the fan operates at high speed and high flow volume, there is the impeller that requires low torque and power. The study investigated and compared three types of blades. In the first position for the flexible blade at $\omega = 1500$ rpm and $Q = 7000$ m³/h, the rising pressure, power, and efficiency are 2620,2 Pa, 59,694 kW, and 54,33 %, respectively, equal to the fixed blade 1. In the last position for the flexible blade at $\omega = 3500$ rpm and $Q = 22000$ m³/h, the rising pressure, power, and efficiency are 5708,1 Pa, 94,771 kW, and 36,81 %, respectively, equal to the fixed blade 2. Besides, the CFD results showed that the flexible fan has a significant effective operating range from $\omega = 2161,31$ rpm and $Q = 8775,51$ m³/h to $\omega = 3354,51$ rpm and $Q = 17285,7$ m³/h. In this range, the rising pressure of the flexible blade changes from 5437,2 Pa to 10112 Pa; the power changes from 24,528 kW to 68,181 kW; and the efficiency changes from 54,04% to 73,31%.

In this study, we demonstrated the feasibility of the proposed solution by designing a 3D model, a mathematical model to calculate the blade position at each speed and flow, simulated by Matlab and CFD. The results of the research have also given a concept of a novel centrifugal fan that can effectively meet different operating conditions.

Author Contributions

T.T. Hiep planned the scheme, initiated the project, developed the mathematical modeling, and built the 3D models and simulation; H.D. Thong, L.T. Long, and V.V. Thang consulted for simulation results and made the literature review. The manuscript was written through the contribution of all authors. All authors discussed the results, reviewed, and approved the final version of the manuscript.

Acknowledgments

We acknowledge Ho Chi Minh City University of Technology (HCMUT), VNU-HCM for supporting this study.

Conflict of Interest

The authors declared no potential conflicts of interest concerning the research, authorship, and publication of this article.

Funding

The authors received no financial support for the research, authorship, and publication of this article.

Data Availability Statements

The datasets generated and/or analyzed during the current study are available from the corresponding author on reasonable request.

Nomenclature

b	Impeller width [m]	T_s	The shaft torque input [N.m]
C_1, C_2	The inlet and outlet absolute fluid velocity [m/s]	u_1, u_2	The inlet and outlet peripheral speed [m/s]
C_{m1}, C_{m2}	The radial components of fluid velocity [m/s]	W_1, W_2	The velocity tangential to the blade [m/s]
C_{u1}, C_{u2}	The inlet and outlet peripheral component [m/s]	z	The number of blades
D_1, D_2	The inner and outer diameter of the impeller [m]	α	The angle \overline{OBC} [degree]
I_{BC}	The moment of inertia of the blade [kg.m ²]	β_1, β_2	The inlet and outlet blade angle [degree]





k_s	The spring stiffness [N/m]	Δl	The initial deformation of the spring [m]
P_s	The shaft power input [kW]	δ	The thickness of the blade [m]
Q	The airflow volume [m ³ /h]	θ_0	The initial angle \widehat{BCM} [degree]
r_1, r_2	The inner and outer radius of the impeller [m]	ρ	Fluid density [kg/m ³]
R_b	Blades radius [m]	ω	The velocity of the impeller [rpm]


References


- [1] McPherson, M.J., *Subsurface Ventilation and Environmental Engineering*, Springer, Berlin, 1993.
- [2] Moczko, P., Odyjas, P., Pietrusiak, D., Wieckowski, J., Scholz, P., Dix, M., Osiecki, T., Timmel, T., Kroll, L., Enhancing Efficiency of Industrial Centrifugal Fans Using Blade Adjustment Mechanism, *Energies*, 15(3), 2022, 1-15.
- [3] Odyjas, P., Wieckowski, J., Pietrusiak, D., Moczko, P., Challenges in the Design of a New Centrifugal Fan with Variable Impeller Geometry, *Acta Mechanica et Automatica*, 17(1), 2023, 16–27.
- [4] Ding, H., Chang, T., Lin, F., The Influence of the Blade Outlet Angle on the Flow Field and Pressure Pulsation in a Centrifugal Fan, *Processes*, 8(11), 2020, 1-14.
- [5] Chen, X., Yang, M., Deng, K., Bai, Y., Numerical Analysis of a Centrifugal Fan for a Road Sweeper, *Fluids Engineering Division Summer Meeting*, Hawaii, USA, FEDSM2017-69103, 2017.
- [6] Le, T.L., Nghia, T.T., Thong, H.D., Son, M.H.K., Numerical study of aerodynamic performance and flow characteristics of a centrifugal blower, *International Journal of Intelligent Unmanned Systems*, 11(3), 2023, 396-406.
- [7] Bamberger, K., Belz, J., Carolus, T., Nelles, O., Development, Validation and Application of an Optimization Scheme for Impellers of Centrifugal fans Using CFD-Trained Metamodels, *International Conference on Fan Noise, Aerodynamics, Applications and Systems*, Darmstadt, Germany, 2018.
- [8] Bamberger, K., Carolus, T., Belz, J., Nelles, O., Development, Validation, and Application of an Optimization Scheme for Impellers of Centrifugal Fans Using Computational Fluid Dynamics-Trained Metamodels, *Journal of Turbomachinery*, 142(11), 2020, 1-7.
- [9] Akzhigitov, D., Srymbetov, T., Aldabergen, A., Spitas, C., Structural and Aerodynamical Parametric Study of Truss-Core Gas Turbine Rotor Blade, *Journal of Applied and Computational Mechanics*, 7(2), 2021, 831-838.
- [10] Pholdee, N., Kumar, S., Bureerat, S., Nuantong, W., Dongbang, W., Sweep Blade Design for an Axial Wind Turbine using a Surrogate-assisted Differential Evolution Algorithm, *Journal of Applied and Computational Mechanics*, 9(1), 2023, 217–225.
- [11] Subramanya, S., *Modelling and Simulation of Fan Performance using CFD Group*, Master Thesis, Department of Economic and Industrial Development, Linköping University, Linköping, Sweden, 2015.
- [12] Roffi, M., Ferreira, F.J.T.E., Almeida, A.T.D., Comparison of Different Cooling Fan Designs for Electric Motors, *IEEE International Electric Machines and Drives Conference*, Miami, FL, USA, IEMDC, 2017.
- [13] Aiki, S., Hori, T., Hayashi, M., US Patent No. 3915591, 1975.
- [14] Jackson, S.G., US Patent No. 4547126, 1983.
- [15] Cocks, R.B., Hull, M.R., Golm, J.N.C., Beifus, B.L., Stauffer, Z., Warriner, L.M., US Patent No. 9689264B2, 2017.
- [16] Comsol Multiphysics, *CFD User's Guide*, 2016.
- [17] Carolus, T., *Fans: Aerodynamic Design, Noise Reduction, Optimization*, Springer, Wiesbaden, 2022.
- [18] Selvaraj, T., Hariharasakthisudhan, P., Pandiaraj, S., Sathickbasha, K., Noorani, A.B.M.A., Optimizing the Design Parameters of Radial Tip Centrifugal Blower for Dust Test Chamber Application Through Numerical and Statistical Analysis, *FME Transactions*, 48(1), 2020, 236–245.
- [19] Vince, J., *Mathematics for Computer Graphics, Fifth Edition*, Springer, London, 2017.
- [20] Technical specification Merlin XP Hydrostatic, <https://www.munihire.co.uk/assets/technical-datasheets/scarab/Scarab-Merlin-XP-Hydrostatic-Technical.pdf>.
- [21] Global R3 Air Service Manual, <https://sweeperland.com/wp-content/uploads/2016/10/Global-R3-Service-Manual-Bortek-Industries-Inc-compressed.pdf>.
- [22] Adjusting the Element Size for the Unstructured Mesh Generator, <https://www.comsol.com/model/adjusting-the-element-size-for-the-unstructured-mesh-generator-14439>.
- [23] Thong, H.D., Minh, P.Q., Khai, H.Q., Khoi, T.Q., Performance enhancement of the motorcycle exhaust thermoelectric generator - Optimization of the hot-side heat exchanger configuration, *Case Studies in Thermal Engineering*, 53, 2023, 103616.

ORCID iD

Thai Thanh Hiep  <https://orcid.org/0000-0003-4069-9437>

Le Thanh Long  <https://orcid.org/0000-0001-5238-4171>

Vu Viet Thang  <https://orcid.org/0009-0005-6552-9719>

Hong Duc Thong  <https://orcid.org/0000-0002-8010-5851>



© 2024 Shahid Chamran University of Ahvaz, Ahvaz, Iran. This article is an open access article distributed under the terms and conditions of the Creative Commons Attribution-NonCommercial 4.0 International (CC BY-NC 4.0 license) (<http://creativecommons.org/licenses/by-nc/4.0/>).

How to cite this article: Hiep, T.T., Long, L.T., Thang, V.V., Thong, H.D., Design of Centrifugal Fan with Flexible Blades to Extend the Effective Operating Range in Various Speeds and Mass Flows Based on Numerical Analysis and Statistical Computation, *J. Appl. Comput. Mech.*, xx(x), 2024, 1–18. <https://doi.org/10.22055/jacm.2024.44608.4249>

Publisher's Note Shahid Chamran University of Ahvaz remains neutral with regard to jurisdictional claims in published maps and institutional affiliations.

